https://doi.org/10.5194/tc-2022-103
Preprint. Discussion started: 31 May 2022

The Cryosphere Discussions

Compensating errors in inversions for subglacial bed roughness: same steady state, different dynamic response

Constantijn J. Berends[1], Roderik S. W. van de Wal[1,2], Tim van den Akker[1], William H. Lipscomb[3]

[1] Institute for Marine and Atmospheric research Utrecht, Utrecht University, Utrecht, The Netherlands
[2] Faculty of Geosciences, Department of Physical Geography, Utrecht University, Utrecht, The Netherlands
[3] Climate and Global Dynamics Laboratory, National Center for Atmospheric Research, Boulder, CO, USA

Correspondence to: Tijn Berends (c.j.berends@uu.nl)

Abstract. Subglacial bed roughness is one of the main factors controlling the rate of future Antarctic ice-sheet retreat, and also one of the most uncertain. A common technique to constrain the bed roughness using ice-sheet models is basal inversion, tuning the roughness to reproduce the observed present-day ice-sheet geometry and/or surface velocity. However, many other factors affecting ice-sheet evolution, such as the englacial temperature and viscosity, the surface and basal mass balance, and the subglacial topography, also contain substantial uncertainties. Using a basal inversion technique intrinsically causes any errors in these other quantities, to lead to compensating errors in the inverted bed roughness. Using a set of idealised-geometry experiments, we quantify these compensating errors and investigate their effect on the dynamic response of the ice-sheet to a prescribed forcing. We find that relatively small errors in ice viscosity and subglacial topography require substantial compensating errors in the bed roughness in order to produce the same steady-state ice sheet, obscuring the realistic spatial variability in the bed roughness. When subjected to a retreat-inducing forcing, we find that these different parameter combinations, which per definition of the inversion procedure result in the same steady-state geometry, lead to a rate of ice volume loss that can differ by as much as a factor of two. This implies that ice-sheet models that use basal inversion to initialise their model state can still display a substantial model bias despite having an initial state which is close to the observations.

1 Introduction

One of the most worrying long-term consequences of anthropogenic climate change is sea-level rise due to the retreat of the Greenland and Antarctic ice sheets (Oppenheimer et al., 2019; Fox-Kemper et al., 2021). It is also one of the most uncertain consequences, with the projected sea-level contribution from the Antarctic ice sheet in 2100 under high-warming scenarios ranging from -2.5 cm (the minus sign indicating a sea-level drop) to 17 cm (Seroussi et al., 2020). Ice-dynamical processes are the main contributors to this uncertainty, which is demonstrated in the idealised ABUMIP experiment (Sun et al., 2020), which concerns instantaneous ice-shelf collapse under zero atmospheric or oceanic forcing, thereby eliminating uncertainties in the forcing. In this experiment, modelled sea-level rise differs by a factor of 10 among models, on time scales of a few centuries.

https://doi.org/10.5194/tc-2022-103
Preprint. Discussion started: 31 May 2022

One of the main contributing factors to this ice-dynamical uncertainty is basal sliding, which is controlled by the roughness of the subglacial bed. Sun et al. (2020) showed that a substantial amount of the variance in the ABUMIP model ensemble could be explained by different assumptions about basal sliding, both in terms of the relation between bed roughness, sliding velocity, and basal friction (the "sliding law"), and in terms of the bed roughness itself. These processes are difficult to constrain based on observational evidence; observations of the Antarctic subglacial substrate are virtually non-existent, and direct observations of ice velocity are typically limited to the ice-sheet surface, which contains contributions from both basal sliding and vertical shearing. Since the latter is controlled by the ice viscosity, which too is very uncertain, disentangling the two terms is problematic.

An often-used approach for solving this problem is applying inversion techniques to estimate the bed roughness by matching the observed ice thickness and/or surface velocity. Generally speaking, an inversion is a way to calculate the cause of an observed effect; since most physical problems instead consist of calculating the effect of an observed or postulated cause, this is called the "inverse problem". In the case of basal sliding, the forward problem consists of providing an ice-sheet model with a (spatially variable) value for bed roughness, and calculating the resulting ice-sheet geometry and/or velocity. The inverse problem consists of taking the (observed) geometry and/or velocity, and using that to invert for the bed roughness. Different formulations of this approach exist, which differ in the observations the inversion aims to reproduce (e.g. ice-sheet geometry and/or velocity), and in the mathematical techniques used to perform the inversion. A geometry-based approach was introduced by Pollard and DeConto (2012), and adapts the bed roughness during a forward simulation until the model reaches a steady-state ice geometry that matches the observations. The bed roughness is changed based on the local difference between the modelled and the observed ice thickness; if the ice is too thick (thin), the bed roughness is decreased (increased), based on the idea that a lower (higher) bed roughness leads to increased (decreased) ice flow, and therefore thinning (thickening). This approach has since been adopted, with minor variations, in several ice sheet models, e.g. f.ETISh (Pattyn, 2017), and CISM (Lipscomb et al., 2021). The velocity-based approach is used in e.g. Elmer/ice (Gagliardini et al., 2013) and ISSM (Larour et al., 2012). In this approach, the model is not run forward in time; instead, the geometry is kept fixed, and the bed roughness field is iteratively adapted until the modelled velocity field matches the observations. Typically, more elaborate mathematical techniques are used to update the bed roughness than in the geometry-based approach. Since the velocity-based approach does not aim to produce a stable geometry, it generally leads to a more pronounced model drift compared to the geometry-based approach in forward experiments (Seroussi et al., 2019).

These inversion approaches share the underlying assumption that all ice-sheet properties other than the bed roughness are known accurately enough for such an inversion to be meaningful, i.e. that any differences between the modelled and the observed ice-sheet state are mostly due to errors in the modelled bed roughness, and that those errors can be corrected by applying an inversion. This means that, due to the nature of the inversion procedure, any modelled errors in the other ice-sheet properties will lead to compensating errors in the inverted bed roughness. For example, if the modelled ice viscosity

https://doi.org/10.5194/tc-2022-103
Preprint. Discussion started: 31 May 2022

overestimates the real value, then the modelled ice velocities due to viscous deformation will be too low, and the modelled steady-state ice sheet will be too thick. The inversion procedure will compensate for this mismatch by lowering the bed roughness, increasing the sliding velocities, and thinning the ice, until it once again matches the observed state. This implies that the result of a basal inversion will contain not just (an approximation of) the realistic bed roughness, but also the sum of compensating errors that arise from modelled errors in other ice-sheet quantities.

In this study, we investigate these compensating errors, and how they affect the uncertainty in projections of ice-sheet retreat. As a modelling tool we use the vertically-integrated ice-sheet model IMAU-ICE (Berends et al., 2022), which we describe briefly in Sect. 2.1. In Sect. 2.2 we present a novel variation on the geometry-based inversion approach, which uses a flowline-averaged anomaly method to adapt the bed roughness field. We apply this model set-up to two idealised-geometry ice sheets, which we describe in Sect. 3. In Sect. 4.1, we demonstrate that our novel inversion procedure is capable of reproducing the known bed roughness in settings with freely moving ice margins and/or grounding lines. In Sect. 4.2 we present a series of experiments where we introduce errors in other ice-sheet model components before performing the inversion, which results in an erroneous inverted bed roughness, even though, as a construct of the inversion procedure, the resulting steady-state ice sheet is still similar. In Sect. 4.3 we investigate the effect of these compensating errors on the dynamic response of the ice-sheet to a schematic retreat-inducing forcing. We show that, even though the respective errors in the bed roughness and the other model components compensate each other in terms of steady-state ice-sheet geometry, this is not necessarily the case for the dynamic response. We quantify the difference in ice-sheet models with nearly identical steady-state geometries in their rate of sea-level contribution under a forced retreat of as a result of the compensating errors. We discuss the implications of these findings in Sect. 5.

2 Methodology

2.1 Ice-sheet model

IMAU-ICE is a vertically-integrated ice-sheet model, which has been specifically designed for large-scale, long-term simulations of ice-sheet evolution (Berends et al., 2022). It solves the depth-integrated viscosity approximation (DIVA; Gold berg, 2011; Lipscomb et al., 2019) to the stress balance, which is similar to the hybrid SIA/SSA, but which remains close to the full-Stokes solution at significantly higher aspect ratios (Berends et al., 2022). Proper grounding-line migration is achieved by using a sub-grid friction-scaling scheme, based on the approaches used in PISM (Feldmann et al., 2014) and CISM (Leguy et al., 2021).

For this study, a new sliding law was added to IMAU-ICE, based on the work of Zoet and Iverson (2020). This recent work presents a sliding law based on laboratory experiments, contrasting with previous sliding laws which were based chiefly on theoretical considerations. Here, the basal shear stress τ_b depends on the basal velocity u_b as follows:

https://doi.org/10.5194/tc-2022-103
Preprint. Discussion started: 31 May 2022

$$\tau_b = N \tan\varphi \left(\frac{u_b}{u_b+u_0}\right)^{1/p}. \quad (1)$$

Here, N is the (effective) overburden pressure, and φ is the bed roughness, expressed as a till friction angle. By default, the exponent $p = 3$, and the transition velocity $u_0 = 200\ \mathrm{m\ yr^{-1}}$. At low sliding velocities, this sliding law behaves like a Weertman-type power law, with the basal shear stress approaching zero as the basal velocity approaches zero. At high sliding velocities, the basal shear stress asymptotes to the Coulomb friction limit. This two-regime behaviour agrees with the theoretical considerations underlying previous sliding laws.

2.2 Inversion procedure

For this study, we developed a novel inversion procedure. It is based on the procedure used in CISM (Lipscomb et al., 2021), which in turn is a variation on the geometry-based approach from Pollard and DeConto (2012). In the CISM procedure, as in the Pollard and DeConto approach, the ice-sheet model is run forward in time, and the bed roughness field is adapted based on the difference between the modelled and the target ice-sheet. However, whereas the Pollard and DeConto approach only considers the mismatch in ice thickness, the newest, currently yet unpublished approach used in CISM additionally includes the mismatch in surface velocity, leading to faster convergence (since the velocity responds more quickly to changes in bed roughness than the geometry). We extend this approach by adopting a flowline-averaged, rather than a purely local scheme to calculate the mismatch in terms of ice thickness and velocity. The rationale behind this is that changing the bed roughness at any location will affect the ice geometry and velocity not just at that location, but also upstream and downstream. Reducing the basal roughness at one location will increase the ice velocity along the entire flowline, causing the ice both locally and upstream to become thinner. By including these effects in the inversion procedure, numerical stability is improved, and artefacts arising from differences in the flotation mask between the modelled and the target state are reduced.

Let $\boldsymbol{p} = [x, y]$ be a point on the ice sheet. We divide the flowline passing through $\boldsymbol{p}$ into an upstream part $\boldsymbol{L}_u(\boldsymbol{p}, s)$ and a downstream part $\boldsymbol{L}_d(\boldsymbol{p}, s)$, which can be found by integrating the ice surface velocity field $\hat{\boldsymbol{u}} = \frac{\boldsymbol{u}}{|\boldsymbol{u}|}$:

$$\boldsymbol{L}_u(\boldsymbol{p}, s + ds) = \boldsymbol{L}_u(\boldsymbol{p}, s) - \hat{\boldsymbol{u}}\big(\boldsymbol{L}_u(\boldsymbol{p}, s)\big)ds, \quad (2a)$$

$$\boldsymbol{L}_d(\boldsymbol{p}, s + ds) = \boldsymbol{L}_d(\boldsymbol{p}, s) + \hat{\boldsymbol{u}}\big(\boldsymbol{L}_d(\boldsymbol{p}, s)\big)ds, \quad (2b)$$

$$\boldsymbol{L}_u(\boldsymbol{p}, 0) = \boldsymbol{L}_d(\boldsymbol{p}, 0) = \boldsymbol{p}. \quad (2c)$$

Here, s is the distance along the flowline. In the upstream (downstream) direction, the integral is terminated at s_u (s_d) at the ice divide (ice margin), i.e. when $\boldsymbol{u} = \boldsymbol{0}$ ($H = 0$), so that:

$$\boldsymbol{u}\Big(\boldsymbol{L}_u\big(\boldsymbol{p}, s_u(\boldsymbol{p})\big)\Big) = \boldsymbol{0}, \quad (3a)$$

https://doi.org/10.5194/tc-2022-103
Preprint. Discussion started: 31 May 2022


The Cryosphere Discussions

$$H\left(\boldsymbol{L}_d(\boldsymbol{p}, s_d(\boldsymbol{p}))\right) = 0. \tag{3b}$$

In order to calculate the rate of change $\frac{d\varphi}{dt}$ of the till friction angle φ, the velocity mismatch (defined as the difference between the modelled absolute surface velocity $|\boldsymbol{u}_m|$ and the target absolute surface velocity $|\boldsymbol{u}_t|$) is averaged over both the upstream (Eq. 4a) and downstream (Eq. 4b) part of the flowline, whereas the ice thickness mismatch is evaluated only in the upstream direction (Eq. 4c; preliminary experiments showed that including a downstream ice thickness term was detrimental to the results):

$$I_1(\boldsymbol{p}) = \int_{s=0}^{s_u(\boldsymbol{p})} \left(\frac{|\boldsymbol{u}_m(\boldsymbol{L}_u(\boldsymbol{p},s))| - |\boldsymbol{u}_t(\boldsymbol{L}_u(\boldsymbol{p},s))|}{u_0}\right) w_u\big(s, s_u(\boldsymbol{p})\big) ds, \tag{4a}$$

$$I_2(\boldsymbol{p}) = \int_{s=0}^{s_d(\boldsymbol{p})} \left(\frac{|\boldsymbol{u}_m(\boldsymbol{L}_d(\boldsymbol{p},s))| - |\boldsymbol{u}_t(\boldsymbol{L}_d(\boldsymbol{p},s))|}{u_0}\right) w_d\big(s, s_d(\boldsymbol{p})\big) ds, \tag{4b}$$

$$I_3(\boldsymbol{p}) = \int_{s=0}^{s_u(\boldsymbol{p})} \left(\frac{H_m(\boldsymbol{L}_u(\boldsymbol{p},s)) - H_t(\boldsymbol{L}_u(\boldsymbol{p},s))}{H_0}\right) w_u\big(s, s_u(\boldsymbol{p})\big) ds. \tag{4c}$$

The default values for the scaling parameters are $u_0 = 250$ m yr^{-1}, $H_0 = 100$ m. The linear scaling functions w_u, w_d serve to assign more weight to anomalies close to $\boldsymbol{p}$, decreasing to zero at the respective ends of the flowline, as well as to normalise the integral:

$$w_u\big(s, s_u(\boldsymbol{p})\big) = \frac{2}{s_u(\boldsymbol{p})}\left(1 - \frac{s}{s_u(\boldsymbol{p})}\right), \tag{5a}$$

$$w_d\big(s, s_d(\boldsymbol{p})\big) = \frac{2}{s_d(\boldsymbol{p})}\left(1 - \frac{s}{s_d(\boldsymbol{p})}\right). \tag{5b}$$

The scaling functions are constructed such that $\int_{s=0}^{s=s_u(\boldsymbol{p})} w_u ds = \int_{s=0}^{s=s_d(\boldsymbol{p})} w_d ds = 1$. The three line integrals from Eqs. 4a-c are then added together, and scaled with the local ice thickness $H(\boldsymbol{p})$ and velocity $|\boldsymbol{u}(\boldsymbol{p})|$. This reflects the fact that bed roughness underneath slow-moving, thin ice has less effect on the large-scale ice-sheet geometry than the roughness underneath fast-flowing, thick ice:

$$I_{\text{tot}}(\boldsymbol{p}) = \big(I_1(\boldsymbol{p}) + I_2(\boldsymbol{p}) + I_3(\boldsymbol{p})\big) R(\boldsymbol{p}), \tag{6}$$

$$R(\boldsymbol{p}) = \frac{|\boldsymbol{u}(\boldsymbol{p})| H(\boldsymbol{p})}{u_s H_s}, 0 \le R(\boldsymbol{p}) \le 1. \tag{7}$$

https://doi.org/10.5194/tc-2022-103
Preprint. Discussion started: 31 May 2022

By default, the scaling parameters are $u_s = 3{,}000$ m yr^{-1}, $H_s = 300$ m. The values are based on preliminary experiments to attain fast converge without creating unwanted numerical artefacts. Finally, the rate of change $\frac{d\varphi}{dt}$ of the till friction angle φ can be calculated:

$$\frac{d\varphi(\boldsymbol{p})}{dt} = -\frac{\varphi(\boldsymbol{p}) I_{\mathrm{tot}}(\boldsymbol{p})}{\tau}. \quad (8)$$

The default value for the time scale is $\tau = 10$ yr, again based on preliminary experiments to balance the convergence rate against the numerical stability of the procedure. While the flowline integrals in Eqs. 4a-c are calculated over the entire flowline (including floating ice), $\frac{d\varphi}{dt}$ is calculated only for grounded ice; it is then extrapolated to fill the entire model domain using a simple Gaussian kernel. This approach helps to prevent artefacts in grid cells that switch over time between grounded and floating, or ice-covered and ice-free states.

The routine performing these calculations is run asynchronously from the other components of the ice-sheet model, with a time step of $\Delta t_\varphi = 5$ yr. The till friction angle is updated every time this routine is called:

$$\varphi_{n+1} = F_2\left(\varphi_n + \Delta t_\varphi F_1\left(\frac{d\varphi}{dt}\right)\right). \quad (9)$$

Here, F_1 and F_2 are Gaussian smoothing filters, with their respective radii defined relative to the grid resolution: $\sigma_1 = \frac{\Delta x}{1.5}$, $\sigma_2 = \frac{\Delta x}{4}$. This regularisation of the bed roughness serves to prevent overfitting.

It might be possible to improve upon the inversion procedure presented here, achieving faster or more robust convergence, or better computational performance. For example, our flowline-averaged approach might be difficult to implement in parallel models with a distributed-memory architecture (i.e., where a processor might not have access to all the data on a flowline), which is not the case in IMAU-ICE. However, the aim of this manuscript is not to find the most efficient way to perform a basal inversion, but rather to investigate the uncertainties that remain in the result of that inversion even when the procedure itself works perfectly.

2.3 Perfect-model approach

In order to quantify the compensating errors from one particular model component, we use what we call a perfect-model approach. We first use the ice-sheet model to calculate the steady-state ice-sheet geometry for a known bed roughness field in a simulation we call the "target run". The known bed roughness will be called the target roughness, and the resulting ice-sheet

https://doi.org/10.5194/tc-2022-103
Preprint. Discussion started: 31 May 2022

the target geometry. If we then apply the inversion routine, with all model parameters set to the same values as were used to create the target geometry, then theoretically the resulting inverted bed roughness (which we call the unperturbed roughness) should be exactly the same as the target roughness. The difference between the unperturbed roughness and the target roughness is the model error of the inversion routine. If the inversion procedure works adequately, this error should be small.

We then perform a "perturbed" inversion, where we change one or more of the model parameters/components (e.g. viscosity, SMB, subglacial topography) with respect to the target run. As long as the change is small enough that its effect on the steady-state geometry can be compensated for by a change in bed roughness, the inversion will produce a geometry that still matches the target geometry, but with a different bed roughness, which we call the perturbed roughness. The difference between the perturbed and unperturbed roughness is the compensating error in the bed roughness caused by the error in the model parameter that was changed in the perturbed run. This procedure is illustrated schematically in Fig. 1.

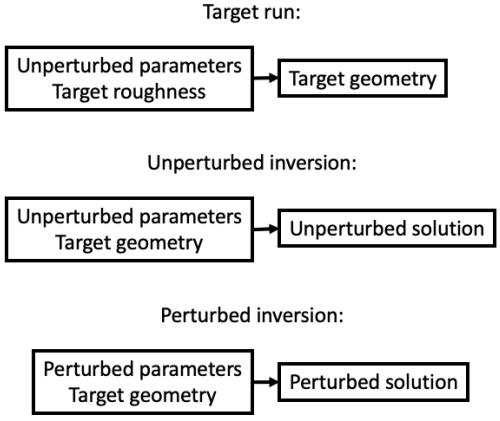

Figure 1: Schematic illustration of the perfect-model approach used in this study.

3 Idealised-geometry ice sheets

3.1 Experiment I: radially symmetrical ice sheet

The first of our two idealised-geometry ice sheets is based on the EISMINT-1 "moving margin" experiment (Huybrechts et al., 1996). It describes an ice-sheet on an infinite, non-deformable flat bed, with a radially symmetrical surface mass balance which is independent of the ice-sheet geometry:

$$M(r) = \min\left(M_{\max}, S(E - r)\right). \tag{10}$$

The values of the parameters are listed in Table 1; the radial distance r from the grid centre is expressed in metres. The ice viscosity is described by a uniform value of Glen's flow law factor A (i.e. no thermomechanical coupling). Lastly, we introduce a non-uniform till friction angle:

$$\varphi(x,y) = \varphi_{\max} - (\varphi_{\max} - \varphi_{\min}) e^{\frac{-1}{2}\left(\left(\frac{x-x_c}{\sigma_x}\right)^2 + \left(\frac{y-y_c}{\sigma_y}\right)^2\right)}. \tag{11}$$

https://doi.org/10.5194/tc-2022-103
Preprint. Discussion started: 31 May 2022

The values of the parameters listed in Table 1.

Table 1: Parameter values for experiment I.

Parameter	Value	Description
$M_{\max}$	0.5 m yr^{-1}	Maximum accumulation rate
E	400 km	Radius of accumulation zone
S	10^{-5} yr^{-1}	Melt rate increase over radial distance from grid centre
A	10^{-16} Pa^{-3} yr^{-1}	Glen's flow law factor
$\varphi_{\min}$	0.1°	Till friction angle in the centre of the ice stream
$\varphi_{\max}$	5°	Till friction angle outside of the ice stream
x_c	0 m	x-coordinate of ice-stream centre
y_c	-400 km	y-coordinate of ice-stream centre
σ_x	50 km	x-direction ice-stream half-width
σ_y	300 km	y-direction ice-stream half-width

The equation thus describes a strip of reduced bed roughness running along the negative y-axis of the domain, which results in the formation of an ice stream with higher ice velocities, and a protruding ice lobe, as illustrated in Fig. 2.

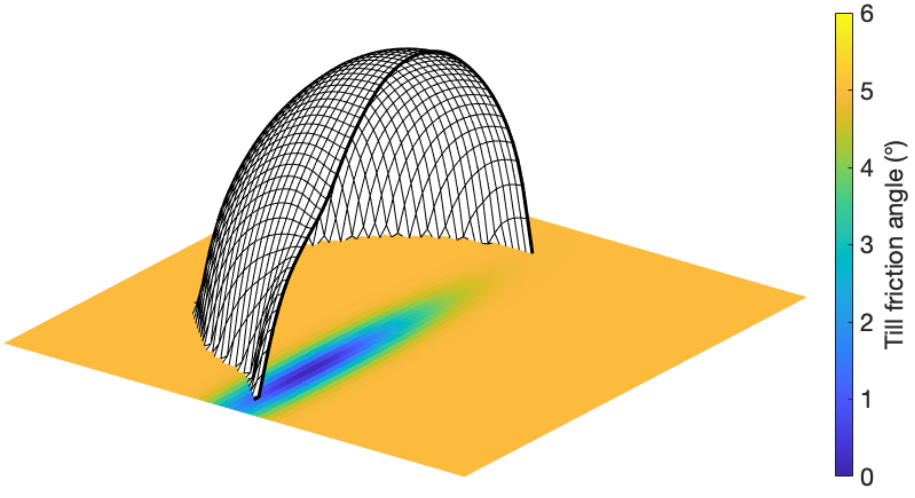

Figure 2: Bed roughness and steady-state ice-sheet geometry in the EISMINT-based experiment I. Black lines on the ice surface are just for illustration. They do not correspond to the model grid.

3.2 Experiment II: laterally symmetrical ice stream with shelf

The second of our two idealised-geometry ice sheets is based on the MISMIP+ geometry (Asay-Davis et al., 2016). This describes a laterally symmetric glacial valley, about 800 km long and 80 km wide, with a slightly over-deepening bed, followed

https://doi.org/10.5194/tc-2022-103
Preprint. Discussion started: 31 May 2022

by a sill, before dropping sharply into a deep oceanic trough. A uniform accumulation rate of 0.3 m yr^{-1} leads to the formation of a fast-flowing ice stream, feeding into a small embayed shelf. The grounding line rests on a retrograde slope, kept in place by buttressing forces. As in experiment I, we introduce a non-uniform bed roughness, which is again described by Eq. 11; the parameters for this experiment are listed in Table 2. Following the MISMIP+ protocol set out by Asay-Davis et al. (2016), the uniform value for Glen's flow law factor A is tuned to achieve a steady-state geometry with a mid-stream grounding-line position at $x = 450$ km, in the middle of the retrograde-sloping part of the bed. The resulting ice-sheet geometry is illustrated in Fig. 3.

Table 2: Parameter values for experiment II.

Parameter	Value	Description
$\varphi_{\min}$	1°	Till friction angle in the centre of the ice stream
$\varphi_{\max}$	5°	Till friction angle outside of the ice stream
x_c	-50 km	x-coordinate of ice-stream centre
y_c	0 km	y-coordinate of ice-stream centre
σ_x	150 km	x-direction ice-stream half-width
σ_y	15 km	y-direction ice-stream half-width

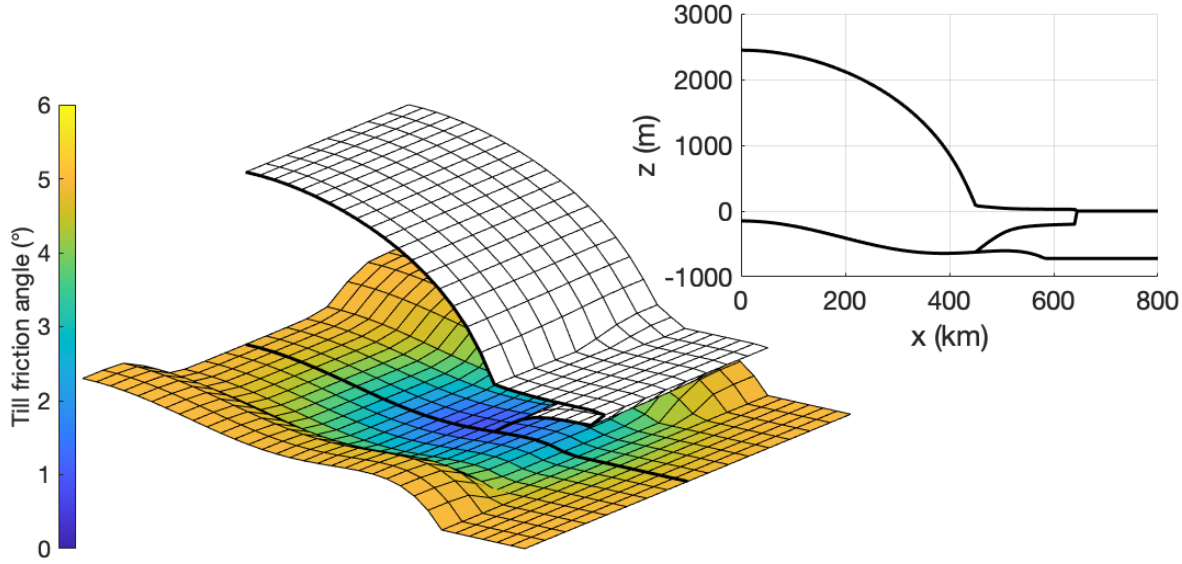

Figure 3: Bed roughness and steady-state ice-sheet geometry in the MISMIP+-based experiment II. Black lines on the ice surface are only for illustration. They do not correspond to the model grid. The top-right panel shows a transect at y = 0, along the central flowline.

https://doi.org/10.5194/tc-2022-103
Preprint. Discussion started: 31 May 2022

4 Results

4.1 Unperturbed inversions

In order to verify that our novel inversion procedure is working properly, we first apply it to both idealised-geometry experiments with all model parameters kept unchanged. The till friction angle is initialised with a uniform value of $\varphi = 5°$, and run forward in time for 100,000 yr. For experiment I, we perform these unperturbed inversions at resolutions of 40, 20, and 10 km; for experiment II we use values of 5 km and 2 km. The resulting inverted bed roughness fields for both sets of simulations are shown in Figs. 4 and 5, respectively. The errors in the inverted bed roughness, and the resulting ice-sheet geometry and velocity, are very small, at all resolutions and in both experiments, indicating that our novel inversion procedure works well in the relatively simple geometries of these two experiments.

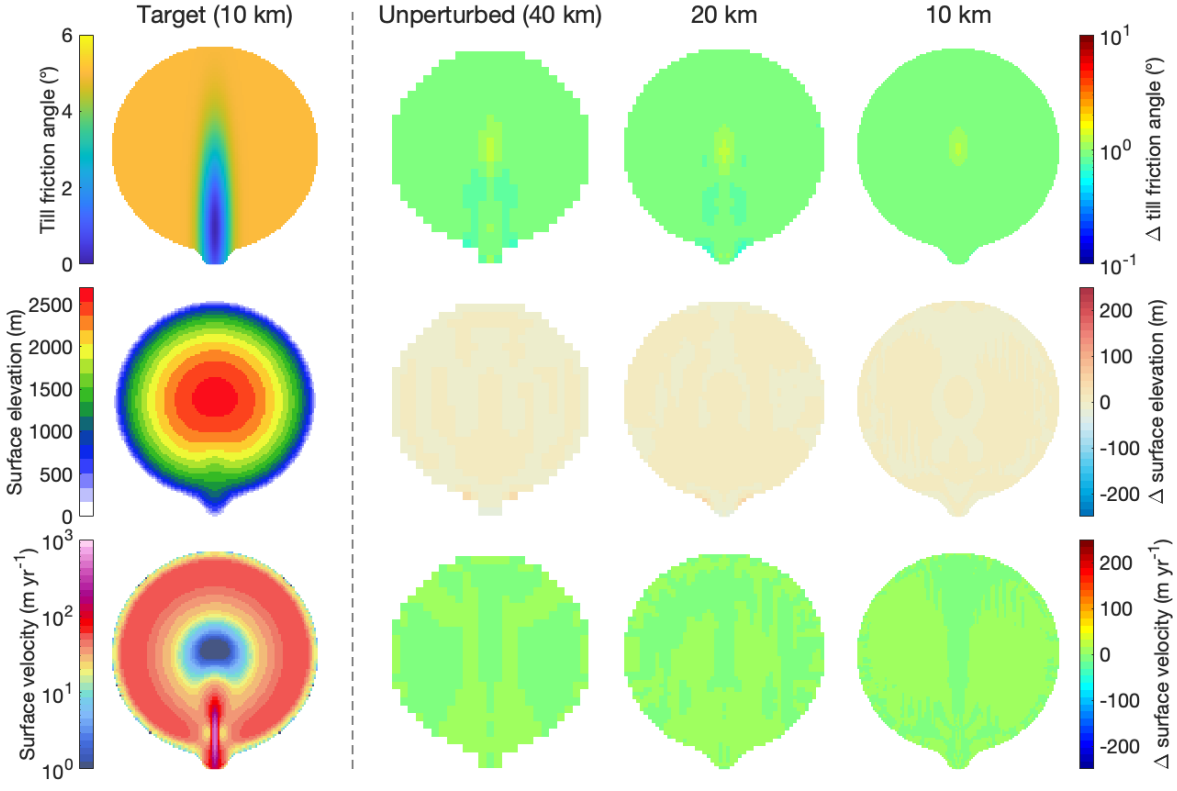

Figure 4: Unperturbed inverted bed roughness, ice-sheet geometry, and ice velocity in experiment I at different resolutions, compared to the target. Top row: till friction angle; middle row: surface elevation; bottom row: surface velocity. For the target run (first column), absolute values are shown (colour scales on the left); for the three unperturbed inversions (second – fourth columns), errors with respect to the target are shown (colour scales on the right). For the till friction angle, the ratio between the inverted and the target value is shown, using a logarithmic colour scale.

https://doi.org/10.5194/tc-2022-103
Preprint. Discussion started: 31 May 2022

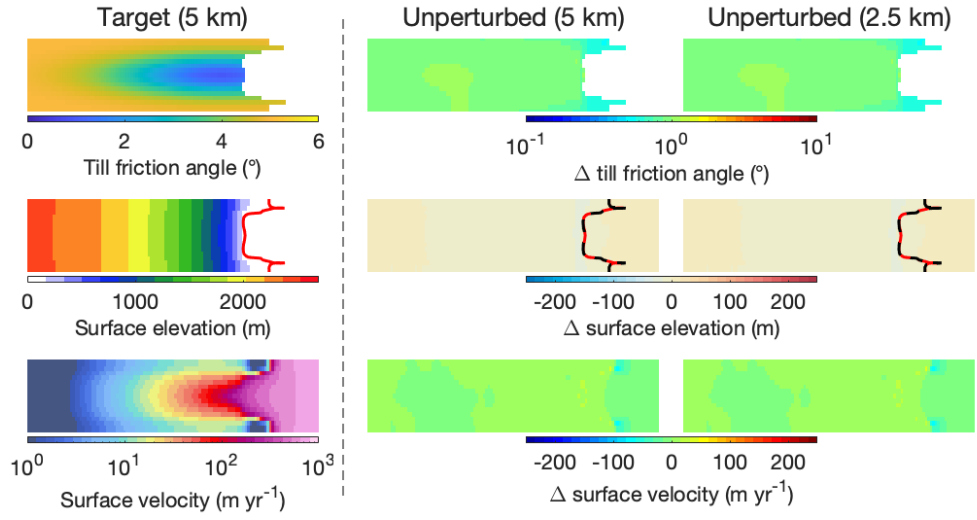

Figure 5: Unperturbed inverted bed roughness, ice-sheet geometry, and ice velocity in experiment II at different resolutions, compared to the target. Top row: till friction angle; middle row: surface elevation; bottom row: surface velocity. For the target run (first column), absolute values are shown; for the three unperturbed inversions (second and third columns), errors with respect to the target are shown. The grounding line in the target (inverted) geometry is indicated by a solid red (dashed black) line.

4.2 Perturbed inversions

To quantify the compensating errors in the inverted bed roughness, we perform a number of perturbed inversions, where we introduce errors in several model components. We increased (decreased) the uniform Glen's flow law factor A by a factor of 1.25; we increased (decreased) the SMB by a factor of 1.05; we increased (decreased) the transition velocity u_0 in the Zoet-Iverson sliding law by a factor of 2; and we increased (decreased) the exponent p in the sliding law by 2. We also performed two perturbed inversions where we added an error to the bed topography of (minus) 10 % of the ice thickness, resulting in a bump (depression) just over 250 m high (deep) underneath the ice divide. The ice thickness was adjusted accordingly to keep the surface elevation unchanged. These five parameters (viscosity, SMB, transition velocity, exponent, topography), each with a high and a low value, result in 10 perturbed inversion simulations. The resulting errors in the inverted bed roughness, steady-state ice geometry, and surface velocity for experiment I are shown in Fig. 6.

https://doi.org/10.5194/tc-2022-103
Preprint. Discussion started: 31 May 2022

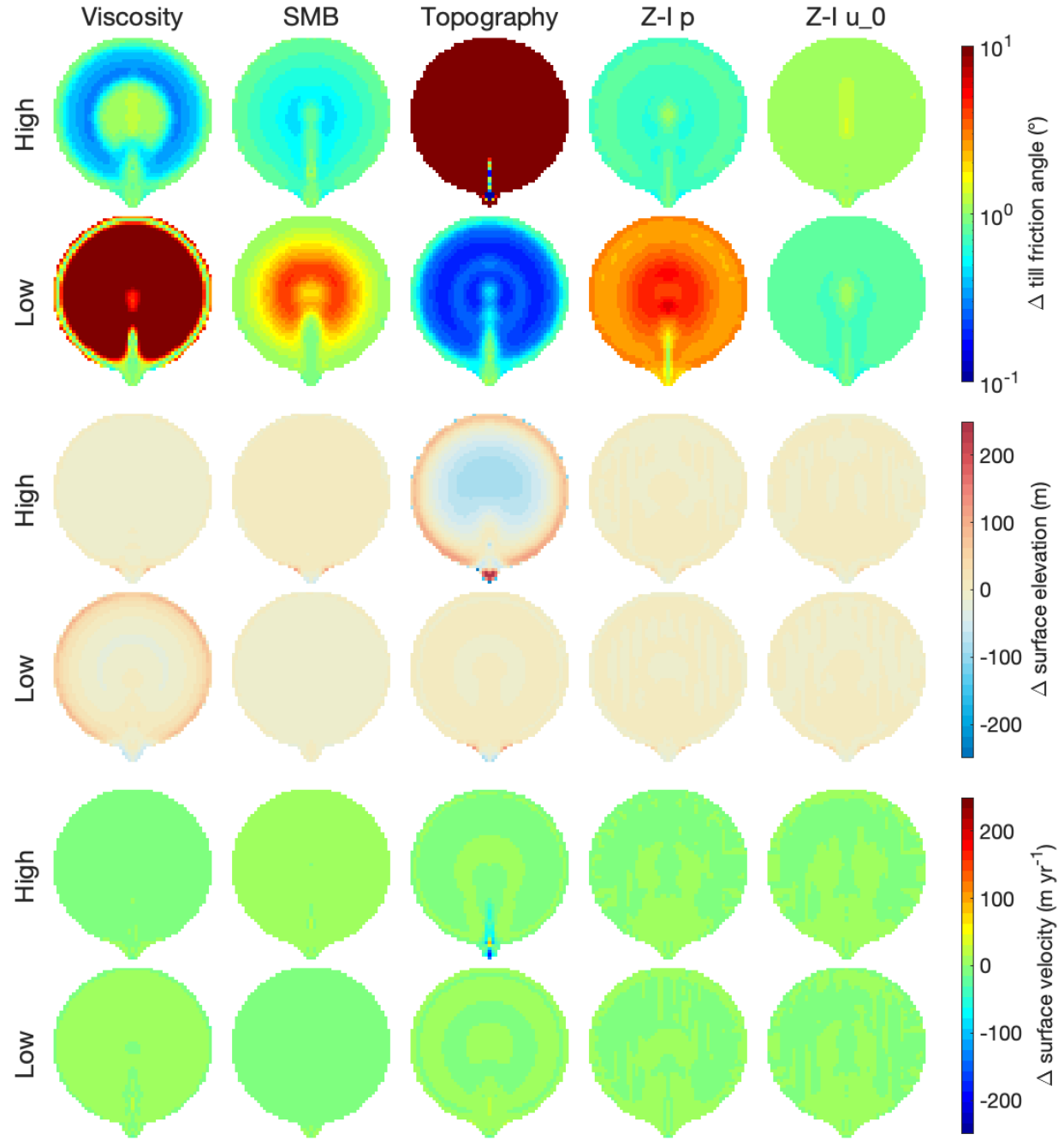

Figure 6: Errors in inverted bed roughness and steady-state ice geometry (relative to the target) for the perturbed inversions of experiment I. The top two rows show the errors in the bed roughness for the high and low perturbed inversions; the middle two rows show the errors in the steady-state surface elevation; and the bottom two rows show the errors in the surface velocity. Each column represents a single perturbed model parameter: viscosity (i.e. Glen's flow law factor A), surface mass balance, subglacial topography, and the exponent p and transition velocity u_0 in the Zoet-Iverson sliding law.

https://doi.org/10.5194/tc-2022-103
Preprint. Discussion started: 31 May 2022

The top-leftmost panel in Fig. 6 shows the error in the inverted bed roughness for the high-viscosity perturbed inversion. In this experiment, the overestimated ice viscosity means that the ice flow due to vertical shearing is underestimated, which is compensated for by decreasing the bed roughness, leading to increased basal sliding. The leftmost panels in the third and fifth row of Fig. 6 show the errors in the resulting steady-state ice geometry and surface velocity, which are negligibly small. In terms of these two quantities, the errors in the viscosity and the bed roughness are indeed compensating errors. This is true for almost all perturbed inversions, except for the low-viscosity and high-topography runs (high-topography means an added depression in the bedrock, such that the target ice thickness is overestimated). In these two experiments, the added perturbations cause the deformational ice flow to be overestimated so much that even preventing all basal sliding cannot entirely compensate for this perturbation. Note that this results from perturbing Glen's flow law factor A by a factor of 1.25, which is rather conservative. In realistic applications, the uncertainty in this quantity is typically an order of magnitude. The choice for this relatively small perturbation was motivated simply by the desire to still achieve a reasonable inverted ice geometry.

The underestimated value of the Zoet-Iverson sliding law exponent $p = 1$ (Fig. 6, fourth column, lower set of rows), which implies a linear sliding law, yields negligible errors in the geometry and velocity, but results in the inverted bed roughness being overestimated by a factor of 3 on average. The overestimated value of $p = 5$ yields negligible differences, as do both over- and underestimated values of the transition velocity u_0.

Even in the remaining four perturbed viscosity / mass balance / topography simulations where the errors in the inverted geometry are acceptably small, the errors in the inverted bed roughness are as large or larger than the "signal" of the prescribed bed roughness pattern (i.e. ~5° of till friction angle change in the ice-stream area). These errors show prominent spatial patterns, despite the fact that the perturbations are spatially uniform. This implies that one should be cautious when interpreting the spatial patterns yielded by a basal inversion procedure, as they are as likely to be the result of errors in some other physical quantity, as they are to reflect realistic variations in bed roughness.

For experiment II, we performed the same set of perturbed inversions as for experiment I, introducing perturbations to the ice viscosity, the surface mass balance, the subglacial topography, and the sliding law parameters. We additionally perturbed the basal mass balance, applying values of ± 1 m/yr (in the target run, no basal melt is applied). The results of the perturbed inversions are shown in Fig. 7. The results of the perturbed Zoet-Iverson sliding law transition velocity u_0 are omitted, since that has only a small effect. Similar to experiment I, the relatively small introduced errors in the ice viscosity, mass balance, and subglacial topography lead to relatively large errors in the inverted bed roughness, but still produce a steady-state ice geometry that is close to the target geometry. The only exceptions are, again, the low-viscosity and high-topography runs, as well as the low-BMB run (i.e. too much sub-shelf melt), where the ice flow is increased more than can be compensated for by increasing the basal friction. However, even here the errors in the inverted geometry are relatively small. The errors in the inverted velocities are mostly small, except for the perturbed basal melt rate inversions. While these produce relatively accurate

https://doi.org/10.5194/tc-2022-103
Preprint. Discussion started: 31 May 2022

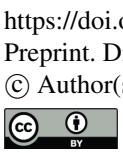

300 geometries (about 120 m of ice loss near the grounding line in the increased-melt simulations), they contain large errors in the shelf velocities (about -500 m/yr in the increased-melt simulation, relative to a target value of about 1,000 m/yr).

As in experiment I, the introduced perturbations (which are spatially uniform) lead to prominent spatial patterns in the inverted bed roughness, with the errors being as large as the actual (prescribed) signal. This underlines the conclusion that spatial
305 patterns in an inverted bed roughness product do not necessarily correspond to spatial patterns in the true bed roughness.

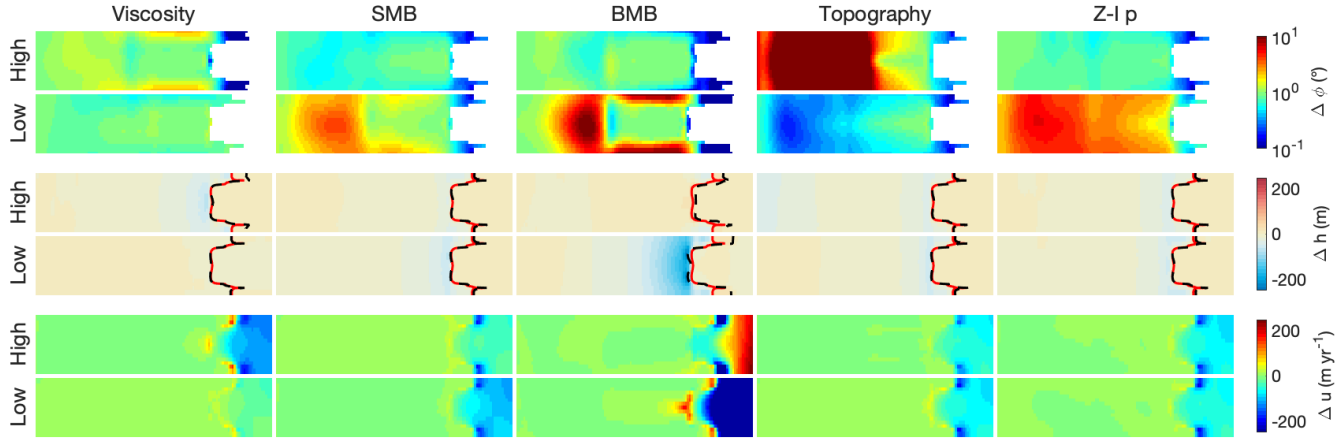

Figure 7: Errors in inverted bed roughness and steady-state ice geometry (relative to the target) for the perturbed inversions of experiment II. The top two rows show the errors in the bed roughness for the high and low perturbed inversions; the middle two rows show the errors in the steady-state surface elevation; and the bottom two rows show the errors in the surface velocity. Each
310 **column represents a single perturbed model parameter: viscosity (i.e. Glen's flow law factor A), surface mass balance, basal mass balance, subglacial topography, and the Zoet-Iverson sliding law exponent *p*. The grounding line in the target (inverted) geometry is indicated by a solid red (dashed black) line.**

Finally, we performed a perturbed inversion where we chose a non-equilibrated target geometry (achieved by terminating the target spin-up simulation after 10,000 yr instead of the default 100,000 yr, such that the ice has only reached about 90 % of its
315 steady-state thickness). Since the present-day observed geometry of the Antarctic ice sheet likely does not represent a steady state, this experiment mimics the effects of erroneously assuming that the ice sheet is in equilibrium (a common assumption in modelling studies). The results of this experiment are shown in Fig. 8. Here too, the inversion procedure results in very small errors in the ice geometry, relatively small errors in the velocity, but substantial errors in the bed roughness.

https://doi.org/10.5194/tc-2022-103
Preprint. Discussion started: 31 May 2022

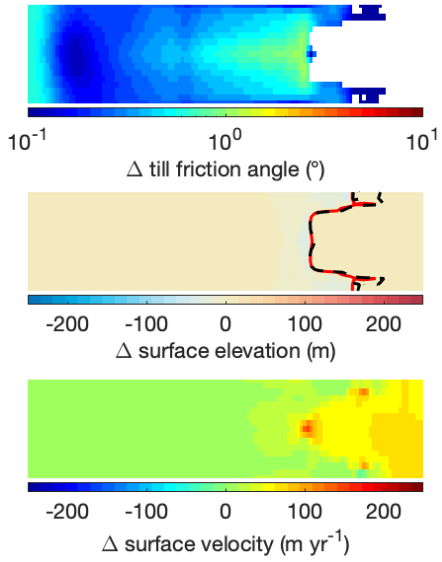

Figure 8: Errors in inverted bed roughness (top), steady-state ice geometry (middle), and surface velocity (bottom) for the non-equilibrium target inversion. The grounding line in the target (inverted) geometry is indicated by a solid red (dashed black) line.

4.3 Dynamic ice-sheet response

To investigate the effect of compensating errors in basal inversions on the dynamic response of the ice sheet, we perform a series of simulations based on experiment II, where we increase the basal melt, forcing the ice sheet to retreat. We use the schematic basal melt parameterisation from the MISMIP+ ice1r experiment (Asay-Davis et al., 2016), and run the model for 500 years. We initialise our simulations with the perturbed parameters, inverted bed roughness, and steady-state ice geometry from the perturbed inversions presented in Sect. 4.2. The resulting ice volume above flotation (relative to the steady state at t = 0) and grounding-line position over time are shown in Fig. 9.

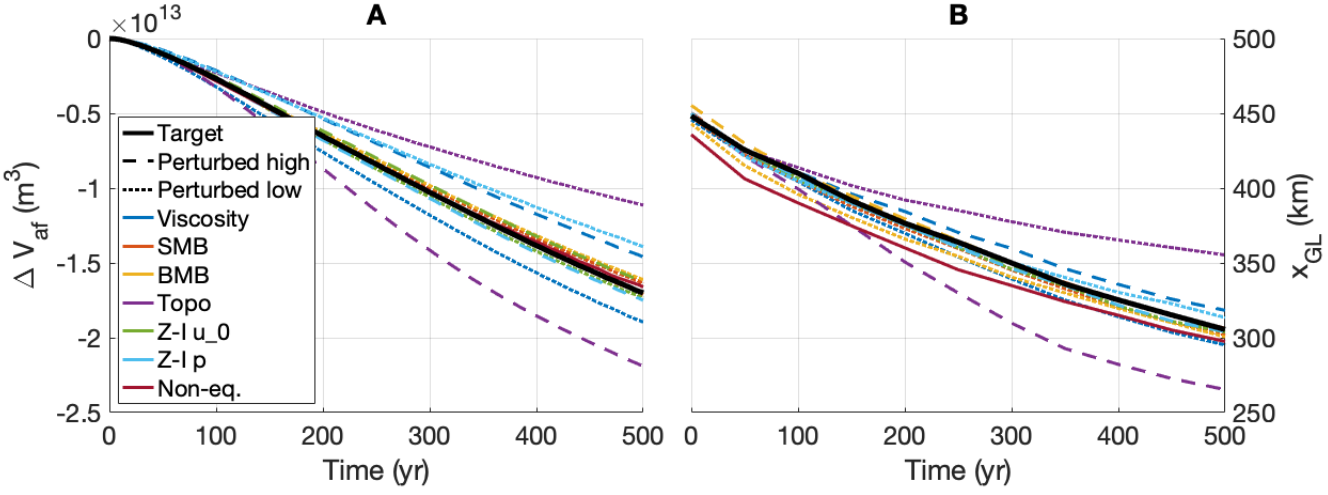

https://doi.org/10.5194/tc-2022-103
Preprint. Discussion started: 31 May 2022

Figure 9, panel A: change in ice volume above flotation (ΔV_{af}), and panel B: grounding-line position (x_{GL}) over time in the perturbed retreat simulations of experiment II. Colours indicate the perturbed parameter; line styles indicate the direction of perturbation. The unperturbed simulation is shown by the solid black line.

In the 500-year unperturbed simulation, the grounding line retreats by about 150 km, causing the ice volume above flotation to decrease by about 1.7 x 10^{13} m^3. As a result of the introduced errors in the perturbed simulations, this mass loss is increased (decreased) by up to 30 % (35 %) relative to the unperturbed simulation. The errors in the subglacial topography have the strongest effect, with the high-perturbed run showing nearly twice as much ice loss as the low-perturbed run. This is followed by the sliding law exponent (-18 % to +3 %) and the ice viscosity (-14 % to +11 %). The effects of the errors in the SMB, the BMB, the sliding law transition velocity, and the non-equilibrated target geometry are negligibly small.

5 Conclusions

We have investigated the effects of compensating errors in basal inversions. We have presented a novel geometry/velocity-based inversion procedure, which produces good results in schematic experiments with a moving ice margin and grounding line. We have applied this method to two different idealised-geometry experiments, where we quantified the errors in the inverted bed roughness that arise from perturbations in other model parameters, such as the ice viscosity, mass balance, sliding law, and subglacial topography. We find that relatively small perturbations in these parameters can lead to substantial compensating errors in the bed roughness. In our idealised experiments, these errors were often larger than the actual spatial variations in bed roughness. This implies that one should be cautious in interpreting the outcome of a basal inversion as an accurate physical representation of bed roughness underneath an ice sheet.

The aim of basal inversion procedures in many ice-sheet models is not to provide an accurate approximation of the actual bed roughness, but rather to produce an ice-sheet that matches the observed state in terms of geometry and/or velocity. The underlying assumption is that any compensating errors in the inverted bed roughness and other model components in terms of the ice geometry, will also compensate each other in terms of their effect on the ice sheet's dynamic response. We tested this assumption by using a basal inversion to initialise a number of different ice-sheet models, all with slightly different model parameters (viscosity, mass balance, etc.). We find that, even though the inversion results in all models have nearly identical steady state geometries, their dynamic response (represented here by the ice volume loss after a short period of forced ice-sheet retreat) can differ by as much as a factor of two. The strongest effect arises from the uncertainty in the subglacial topography, followed by the sliding law exponent and the ice viscosity. Uncertainties in the surface and basal mass balance lead to considerable errors in the bed roughness, but have only a small impact on the dynamic response, as does erroneously assuming that the target (i.e. observed) ice-sheet geometry represents a steady state. The cause of this discrepancy (i.e., why some processes affect both the bed roughness and the dynamical response, but others affect only the roughness but not the response) is not clear.

https://doi.org/10.5194/tc-2022-103
Preprint. Discussion started: 31 May 2022

The geometry of the experiment used to produce these findings describes a marine setting typical of West Antarctica, where the rate of mass loss under a forced retreat is mainly governed by ice-dynamical processes such as viscous flow and basal sliding. In a land-based setting more typical of the Greenland ice sheet, where most mass is lost through atmospheric processes, the effects of these ice-dynamical uncertainties will likely be smaller. However, as long-term projections of sea-level rise under strong warming scenarios are dominated by marine-grounded ice loss in West Antarctica, such projections will likely contain substantial uncertainties as a result of the processes we described, possibly as large as 35 % of the projected ice loss.

Our results imply that, even when basal inversion is used to achieve a stable ice sheet with the desired geometry, uncertainties in other model parameters can have a substantial effect on that ice sheet's dynamic response. Improving our knowledge of the ice sheet interior (temperature, rheology, viscosity) and substrate (geometry, roughness) therefore should remain important goals of the glaciological community.

Acknowledgements. We would like to thank Jorge Bernales and Willem Jan van den Berg for providing helpful comments during the execution of this project.

Author contributions. CJB performed the experiments and analysed the data. CJB wrote the draft of the manuscript; all authors contributed to the final version.

Code and data availability. The source code of IMAU-ICE, scripts for compiling and running the model on a variety of computer systems, and the configuration files for all simulations presented here, are freely available on Github: https://github.com/IMAU-paleo/IMAU-ICE.

Competing interests. The authors declare that they have no competing interests.

Financial support. CJB was supported by PROTECT. This project has received funding from the European Union's Horizon 2020 research and innovation programme under grant agreement no. 869304 (PROTECT; [PROTECT article number will be assigned upon acceptance for publication!]). TvdA was supported by the Netherlands Polar Program. The use of supercomputer facilities was sponsored by NWO Exact and Natural Sciences. Model runs were performed on the Dutch National Supercomputer Snellius. we would like to acknowledge SurfSARA Computing and Networking Services for their support.

References

Asay-Davis, X. S., Cornford, S. L., Durand, G., Galton-Fenzi, B. K., Gladstone, R. M., Gudmunsson, G. H., Hattermann, T., Holland, D. M., Holland, D., Holland, P. R., Martin, D. F., Mathiot, P., Pattyn, F., and Seroussi, H.:

https://doi.org/10.5194/tc-2022-103
Preprint. Discussion started: 31 May 2022

395 Experimental design for three interrelated marine ice sheet and ocean model intercomparison projects: MISMIP v. 3 (MISMIP+), ISOMIP v. 2 (ISOMIP+) and MISOMIP v. 1 (MISOMIP1), Geoscientific Model Development 9, 2471-2497, 2016.

Berends, C. J., Goelzer, H., Reerink, T. J., Stap, L. B. and van de Wal., R. S. W.: Benchmarking the vertically integrated ice-sheet model IMAU-ICE (version 2.0), Geoscientific Model Development Discussions, 2021b, *under review*.

400 Feldmann, J., Albrecht, T., Khroulev, C., Pattyn, F., and Levermann, A.: Resolution-dependent performance of grounding line motion in a shallow model compared with a full-Stokes model according to the MISMIP3d intercomparison, Journal of Glaciology 60, 353-360, 2014.

Fox-Kemper, B., H. T. Hewitt, C. Xiao, G. Adalgeirsdottir, S.S. Drijfhout, T.L. Edwards, N.R. Golledge, M. Hemer, R.E. Kopp, G. Krinner, A. Mix, D. Notz, S. Nowicki, I.S. Nurhati, L. Ruiz, J-B. Sallée, A.B. A. Slangen, Y. Yu, Ocean,

405 Cryosphere and Sea Level Change. Climate Change 2021: The Physical Science Basis. Contribution of Working Group 1 to the Sixth Assessment Report of the Intergovernmental Panel on Climate change [Masson-Delmotte, V., P. Zhai, A. Pirani, S.L. Connors, C.Péan, S. Berger, N. Caud, Y. Chen, L. Goldfarb, M.I. Gomis, M. Huang, K. Leitzell, E. Lonnoy, J.B.R. Matthes, T.K. Maycock, T. Waterfield, O. Yelekci, R. Yu and B. Zhou (eds.)] (2021).

Goldberg, D. N.: A variationally derived, depth-integrated approximation to a higher-order glaciological flow model,

410 Journal of Glaciology 57, 157-170, 2011.

Huybrechts, P., Payne, T., Abe-Ouchi, A., Calov, R., Fabre, A., Fastook, J. L., Greve, R., Hindmarsh, R. C. A., Hoydal, O., Johannesson, T., MacAyeal, D. R., Marsiat, I., Ritz, C., Verbitsky, M. Y., Waddington, E. D., and Warner, R.: The EISMINT benchmarks for testing ice-sheet models, Annals of Glaciology 23, 1-12, 1996.

Leguy, G. R., Lipscomb, W. H., and Asay-Davis, X. S.: Marine ice sheet experiments with the Community Ice Sheet

415 Model, The Cryosphere 15, 3229-3253, 2021

Larour, E., Seroussi, H., Morlighem, M., and Rignot, E.: Continental scale, high order, high spatial resolution, ice sheet modeling using the Ice Sheet System Model (ISSM), Journal of Geophysical Research 117, doi:10.1029/2011JF002140, 2012

Lipscomb, W. H., Price, S. F., Hoffman, M. J., Leguy, G. R., Bennett, A. R., Bradley, S. L., Evans, K. J., Fyke, J. G.,

420 Kennedy, J. H., Perego, M., Ranken, D. M., Sacks, W. J., Salinger, A. G., Vargo, L. J., and Worley, P. H.: Description and evaluation of the Community Ice Sheet Model (CISM) v2.1, Geoscientific Model Development 12, 387-424, 2019.

Lipscomb, W. H., Leguy, G. R., Jourdain, N. C., Asay-Davis, X. S., Seroussi, H., and Nowicki, S.: ISMIP6-based projections of ocean-forced Antarctic Ice Sheet evolution using the Community Ice Sheet Model, The Cryosphere 15, 633-661, 2021.

425 Oppenheimer, M., Glavovic, B., Hinkel, J., van de Wal, R. S. W., Magnan, A. K., Abd-Elgawad, A., Cai, R., Cifuentes-Jar, R., DeConto, R. M., Ghosh, T., Hay, J., Isla, F., Marzeion, B., Meyssignac, B., Sebesvari, Z.: Sea Level Rise and Implications for Low Lying Islands, Coasts, and Communities, in: IPCC Spe- cial Report on the Ocean and Cryosphere

in a Changing Climate, edited by: Pörtner, H.-O., Roberts, D. C., Masson-Delmotte, V., Zhai, P., Tignor, M., Poloczanska, E., Mintenbeck, K., Nicolai, M., Okem, A., Petzold, J., Rama, B., and Weyer, N., 2019.

Pattyn, F.: Sea-level response to melting of Antarctic ice shelves on multi-centennial timescales with the fast Elementary Thermomechanical Ice Sheet model (f.ETISh v1.0), The Cryosphere 11, 1851-1878, 2017.

Pollard, D. and DeConto, R. M.: A simple inverse method for the distribution of basal sliding coefficients under ice sheets, applied to Antarctica, The Cryosphere 6, 953-971, 2012.

Seroussi, H., Nowicki, S., Simon, E. G., Abe-Ouchi, A., Albrecht, T., Brondex, J., Cornford, S. L., Dumas, C., Gillet-Chaulet, F., Goelzer, H., Golledge, N. R., Gregory, J. M., Greve, R., Hoffman, M. J., Humbert, A., Huybrechts, P., Kleiner, T., Larour, E., Leguy, G. R., Lipscomb, W. H., Lowry, D. P., Mengel, M., Morlighem, M., Pattyn, F., Payne, A. J., Pollard, D., Price, S. F., Quiquet, A., Reerink, T. J., Reese, R., Rodehacke, C., Schlegel, N.-J., Shepherd, A., Sun, S., Sutter, J., Van Breedam, J., van de Wal, R. S. W., Winkelmann, R., and Zhang, T.: initMIP-Antarctica: an ice sheet model initialization experiment of ISMIP6, The Cryosphere 13, 1441-1471, 2019.

Seroussi, H., Nowicki, S., Payne, A. J., Goelzer, H., Lipscomb, W. H., Abe-Ouchi, A., Agosta, C., Albrecht, T., Asay-Davis, X. S., Barthel, A., Calov, R., Cullather, R., Dumas, C., Galton-Fenzi, B. K., Gladstone, R. M., Golledge, N. R., Gregory, J. M., Greve, R., Hattermann, T., Hoffman, M. J., Humbert, A., Huybrechts, P., Jourdain, N. C., Kleiner, T., Larour, E., Leguy, G. R., Lowry, D. P., Little, C. M., Morlighem, M., Pattyn, F., Pelle, T., Price, S. F., Quiquet, A., Reese, R., Schlegel, N.-J., Shepherd, A., Simon, E. G., Smith, R. S., Straneo, F., Sun, S., Trusel, L. D., Van Breedam, J., van de Wal, R. S. W., Winkelmann, R., Zhao, C., Zhang, T., and Zwinger, T.: ISMIP6 Antarctica: a multi-model ensemble of the Antarctic ice sheet evolution over the 21st century, The Cryosphere 14, 3033-3070, 2020.

Sun, S., Pattyn, F., Simon, E. G., Albrecht, T., Cornford, S. L., Calov, R., Dumas, C., Gillet-Chaulet, F., Goelzer, H., Golledge, N. R., Greve, R., Hoffman, M. J., Humbert, A., Kazmierczak, E., Kleiner, T., Leguy, G. R., Lipscomb, W. H., Martin, D., Morlighem, M., Nowicki, S., Pollard, D., Price, S. F., Quiquet, A., Seroussi, H., Schlemm, T., Sutter, J., van de Wal, R. S. W., Winkelmann, R., and Zhang, T.: Antarctic ice sheet response to sudden and sustained ice-shelf collapse (ABUMIP), Journal of Glaciology 66, 891-904, 2020.

Zoet, L. K. and Iverson, N. R.: A slip law for glaciers on deformable beds, Science 368, 76-78, 2020.